Lawrence Berkeley National Laboratory

Title
APPLICATION OF BOREHOLE GEOPHYSICS AT AN EXPERIMENTAL WASTE STORAGE SITE

Permalink
https://escholarship.org/uc/item/9df030w4

Author
Nelson, P.H.

Publication Date
1980-06-01

SWEDISH-AMERICAN COOPERATIVE PROGRAM ON RADIOACTIVE WASTE STORAGE IN MINED CAVERNS IN CRYSTALLINE ROCK

APPLICATION OF BOREHOLE GEOPHYSICS AT AN EXPERIMENTAL WASTE STORAGE SITE

P. H. Nelson, K. A. Magnusson,
and R. Rachiele

Lawrence Berkeley Laboratory
University of California
Berkeley, California 94720

June 1980

A Joint Project of

DISCLAIMER

APPLICATION OF BOREHOLE GEOPHYSICS
AT AN EXPERIMENTAL WASTE STORAGE SITE

P.H. Nelson, K.A. Magnusson, and R. Rachiele

Earth Sciences Division
Lawrence Berkeley Laboratory
University of California
Berkeley, CA 94720

June 1980

PREFACE

This report is one of a series documenting the results of the Swedish-American cooperative research program in which the cooperating scientists explore the geological, geophysical, hydrological, geochemical, and structural effects anticipated from the use of a large crystalline rock mass as a geologic repository for nuclear waste. This program has been sponsored by the Swedish Nuclear Power Utilities through the Swedish Nuclear Fuel Supply Company (SKBF), and the U.S. Department of Energy (DOE) through the Lawrence Berkeley Laboratory.

The principal investigators are L.B. Nilsson and O. Degerman for SKBF, and N.G.W. Cook, P.A. Witherspoon, and J.E. Gale for LBL. Other participants will appear as authors of the individual reports.

Previous technical reports in this series are listed below.

1. Swedish-American Cooperative Program on Radioactive Waste Storage in Mined Caverns by P.A. Witherspoon and O. Degerman. (LBL-7049, SAC-01).

2. Large Scale Permeability Test of the Granite in the Stripa Mine and Thermal Conductivity Test by Lars Lundstrom and Haken Stille. (LBL-7052, SAC-02).

3. The Mechanical Properties of the Stripa Granite by Graham Swan. (LBL-7074, SAC-03).

4. Stress Measurements in the Stripa Granite by Hans Carlsson. (LBL-7078, SAC-04).

5. Borehole Drilling and Related Activities at the Stripa Mine by P.J. Kurfurst, T. Hugo-Persson, and G. Rudolph. (LBL-7080, SAC-05).

6. A Pilot Heater Test in the Stripa Granite by Hans Carlsson. (LBL-7086, SAC-06).

7. An Analysis of Measured Values for the State of Stress in the Earth's Crust by Dennis B. Jamison and Neville G.W. Cook. (LBL-7071, SAC-07).

8. Mining Methods Used in the Underground Tunnels and Test Rooms at Stripa by B. Andersson and P.A. Halen. (LBL-7081, SAC-08).

9. Theoretical Temperature Fields for the Stripa Heater Project by T. Chan, Neville G.W. Cook, and C.F. Tsang. (LBL-7082, SAC-09).

10. Mechanical and Thermal Design Considerations for Radioactive Waste Repositories in Hard Rock. Part I: An Appraisal of Hard Rock for Potential Underground Repositories of Radioactive Waste by N.G.W. Cook; Part II: In Situ Heating Experiments in Hard Rock: Their Objectives and Design by N.G.W. Cook and P.A. Witherspoon. (LBL-7073, SAC-10).

11. Full-Scale and Time-Scale Heating Experiments at Stripa: Preliminary Results by N.G.W. Cook and M. Hood. (LBL-7072, SAC-11).

12. Geochemistry and Isotope Hydrology of Groundwaters in the Stripa Granite: Results and Preliminary Interpretation by P. Fritz, J.F. Barker, and J.E. Gale. (LBL-8285, SAC-12).

13. Electrical Heaters for Thermo-Mechanical Tests at the Stripa Mine by R.H. Burleigh, E.P. Binnall, A.O. DuBois, D.O. Norgren, and A.R. Ortiz. (LBL-7063, SAC-13).

14. Data Acquisition, Handling, and Display for the Heater Experiments at Stripa by Maurice B. McEvoy. (LBL-7063, SAC-14).

15. An Approach to the Fracture Hydrology at Stripa: Preliminary Results by J.E. Gale and P.A. Witherspoon. (LBL-7079, SAC-15).

16. Preliminary Report on Geophysical and Mechanical Borehole Measurements at Stripa by P. Nelson, B. Paulsson, R. Rachiele, L. Andersson, T. Schrauf, W. Hustrulid, O. Duran, and K.A. Magnussen. (LBL-8280, SAC-16).

17. Observations of a Potential Size-Effect in Experimental Determination of the Hydraulic Properties of Fractures by P.A. Witherspoon, C.H. Amick, J.E. Gale, and K. Iwai. (LBL-8571, SAC-17).

18. Rock Mass Characterization for Storage in Nucler Waste in Granite by P.A. Witherspoon, P. Nelson, T. Doe, R. Thorpe, B. Paulsson, J.E. Gale, and C. Forster. (LBL-8570, SAC-18).

19. Fracture Detection in Crystalline Rock Using Ultrasonic Shear Waves by K.H. Waters, S.P. Palmer, and W.F. Farrell. (LBL-7051, SAC-19).

20. Characterization of Discontinuities in the Stripa Granite--Time Scale Heater Experiment by R. Thorpe. (LBL-7083, SAC-20).

21. Geology and Fracture System at Stripa by A. Okliewicz, J.E. Gale, R. Thorpe, and B. Paulsson. (LBL-8907, SAC-21).

22. Calculated Thermally Induced Displacements and Stresses for Heater Experiements at Stripa by T. Chan and N.G.W. Cook. (LBL-7061, SAC-22).

23. Validity of Cubic Law for Fluid Flow in a Deformable Rock Fracture by P.A. Witherspoon, J. Wang, K. Iwai, and J.E. Gale. (LBL-9557, SAC-23).

24. Determination of In-Situ Thermal Properties of Stripa Granite from Temperature Measurements in the Full-Scale Heater Experiments: Methods and Primary Results by J. Jeffry, T. Chan, N.G.W. Cook and P.A. Witherspoon. (LBL-8424, SAC-24).

25. Instrumentation Evaluation, Calibration, and Installation for Heater Tests Simulating Nuclear Waste in Crystalline Rock, Sweden by T. Schrauf, H. Pratt, E. Simonson, W. Hustrulid, P. Nelson, A. DuBois, E. Binnall, and R. Haught. (LBL-8313, SAC-25)

26. Part I: Some Results From a Field Investigation of Thermo-Mechanical Loading of a Rock Mass When Heater Canisters are Emplaced in the Rock by M. Hood. Part II: The Application of Field Data from Heater Experiments Conducted at Stripa, Sweden for Repository Design by M. Hood, H. Carlsson, and P.H. Nelson. (LBL-9392, SAC-26).

27. Progress with Field Investigations at Stripa by P.A. Witherspoon, N.G.W. Cook, and J.E. Gale (LBL-10559, SAC-27).

28. A Laboratory Assessment of the Use of Borehole Pressure Transients to Measure the Permeability of Fractured Rock Masses by C.B. Forster and J.E. Gale. (LBL-8674, SAC-28).

29. Thermal and Thermomechanical Data for In Situ Heater Experiments at Stripa, Sweden by T. Chan, E. Binnall, P. Nelson, O. Wan, C. Weaver, K. Ang, J. Braley, and M. McEvoy. (LBL-11477, SAC-29).

30. The Effect of Radon Transport in Groundwater Upon Gamma Ray Borehole Logs by P.H. Nelson, R. Rachiele, and A. Smith. (LBL-11180, SAC-30).

31. Strength and Permeability Tests on Ultra-Large Stripa Granite Core by R. Thorpe, D.J. Watkins, W.E. Ralph, R. Hsu, and S. Flexser. (LBL-11203, SAC-31).

32. Ultrasonic and Acoustic Emission Results from the Stripa Heater Experiments. Part I: A Cross-Hole Investigation of a Rock Mass Subjected to Heating by B.N.P. Paulsson and M.S. King. Part II: Acoustic Emission Monitoring During Cool-Down of the Stripa Heater Experiment by R. Rachiele. (LBL-10975, SAC-32).

33. Numerical Modeling to Assess Possible Influence of the Mine Openings on Far-Field In Situ Stress Measurements at Stripa by T. Chan, V. Guvanasen, and N. Littlestone (LBL-12469, SAC-33).

34. A Field Assessment of the Use of Borehole Pressure Transients to Measure the Permeability of Fractured Rock Masses by C.B. Forster and J.E. Gale. (LBL-11829, SAC-34).

35. Water Inflow into Boreholes During the Stripa Experiments by P.H. Nelson, R. Rachiele, J.S. Remer and H.S. Carlsson (LBL-12547, SAC-35).

36. Petrology and Radiogeology of the Stripa Pluton by H. Wollenberg, S. Flexser, and L. Andersson. (LBL-11654, SAC-36).

37. Geohydrological Data from the Macopermeability Experiment at Stripa, Sweden by C.R. Wilson, J.C.S. Long, R.M. Galbraith, K. Karasaki, H.K. Endo, A.O. DuBois, M.J. McPherson, and G. Ramqvist. (LBL-12520, SAC-37).

38. Characterization of Discontinuities in the Stripa Granite--Full-Scale Heater Experiments by B.N.P. Paulsson, P.H. Nelson, and P.J. Kurfurst. (LBL-9063, SAC-38).

TABLE OF CONTENTS

LIST OF FIGURES

ABSTRACT

A suite of electrical, mechanical, and radiation-measurement borehole probes were run in a 76-mm-diameter borehole drilled to a slant depth of 380 m in leptite and granite. The hole is located in Precambrian bedrock in central Sweden, where a site is dedicated to in situ experiments pertaining to the disposal of radioactive wastes. The challenge to borehole logging methods for such site investigations is to resolve geological features and fluid flow parameters in sites that will be chosen initially for their homogeneity, low porosity, and minimal fracturing. The Stripa borehole is characterized by high electrical resistivity values in the 20 to 100 kμm range, by acoustic velocities around 5,800 m/s (close to laboratory values on intact specimens), and by total porosity of around one volume percent. In this context, probe resolution was adequate to produce interpretable information on almost all of the logs.

Two principal rock types were encountered in the hole: granite, of quartz monzonitic composition, and leptite. The granite and leptite intercepts are subdivided into units characterized by mafic mineral content, sulphide mineral content, and electrical and radiation properties. Iron-rich zones in the leptite are highly anomalous on the gamma-gamma and neutron logs; thin mafic zones in the granite can also be distinguished. Occurrences of a few percent pyrite are detected by the electrical, gamma-gamma, and neutron logs. Although overall porosity is quite low throughout the hole, analysis of the resistivity and neutron logs indicates that porosity increases by a few volume percent at fracture zones. The differential resistance and caliper probes detect borehole diameter roughness of less than 1 mm, helping confirm acoustic waveform anomalies which are indicative of

fracture zones. Compressional wave transit time and shear wave inter-
ference patterns usually occur coincident with open fractures observed in
core, the correlation being especially good at major fracture zones. Immedi-
ate requirements for this application of borehole geophysics are the need to
increase understanding and experience in fracture detection with the acoustic
probe and to develop the quantitative evaluation of that fraction of porosity
accessible to fluid flow.

1. INTRODUCTION

A Swedish-American cooperative research program commenced in 1977 at the Stripa mine in central Sweden. In this program, cooperating investigators explore the geological, geophysical, geotechnical, geochemical, hydrological, and mechanical effects anticipated from use of a large crystalline rock mass as a repository for nuclear waste (Witherspoon, Cook, and Gale, 1980).

The evaluation of potential sites for radioactive waste repositories places some new demands on the tools and techniques of borehole measurements. The hydrological regime is of primary importance, requiring the measurement of permeability to unusually low levels, since in situ permeabilities in crystalline rocks commonly range as low as 10^{-18} m^2 (Brace, 1980). In crystalline rock, fluid flows along interconnected fractures; hence the detection and characterization of fractures, even very fine fractures of less than 0.1 mm aperture, are important goals for detection by borehole logging. The storage of fluid afforded by pore space is also an important parameter for site characterization; hence the measurement of porosity at porosity levels of 1% is desired. Most logging experience is based on evaluation of lithologic units for the recovery of oil and gas, and to a lesser extent, for minerals. Usually, the objective is to locate significant anomalies of fluid or mineral content. For a repository, however, we seek a geological environment free of any significant perturbations that might in some way injure the long-term integrity of the repository. In this case, the goal of borehole logging is to aid the geologist in defining the geological and mineralogical character of a potential site.

This study in a crystalline rock site is directed towards evaluating different slim-hole logs for the following purposes:

o recognizing and characterizing different rock units specified by bulk physical properties

o detecting mineralization and mineralogical variations

o monitoring variations of porosity or water content in rock

o detecting fractures

Two systems of geophysical borehole logs have been applied in a cored borehole (SBH-1) of 76 mm diameter. One system was applied by Lawrence Berkeley Laboratory (LBL) and the other by the Geological Survey of Sweden (SGU). LBL used the following suite of logs: neutron, gamma-gamma, gamma-ray, sonic, caliper, and temperature; SGU used point resistance, differential resistance, resistivity, spontaneous potential (SP), induced polarization (IP), very-low frequency radio-wave propagation (VLF), and gamma-ray. It is therefore possible to evaluate the performance of a wide variety of logs in crystalline rock. Specifications of the borehole probes are described in the appendix.

The 380-m-long borehole designated SBH-1 (Fig. 1) is drilled at a 45° inclination from the surface towards the test drift of the mine. The borehole alternately penetrates granite and leptite, terminating in granite at an elevation above the underground test site. The Stripa granite is a relatively uniform, massive and medium-grained rock, generally of quartz monzonite composition. The matrix mineralogy is composed of the primary minerals quartz, plagioclase, and microcline, with lesser muscovite, and biotite altered to chlorite. Opaque minerals, garnet, and zircon occur as accessories.
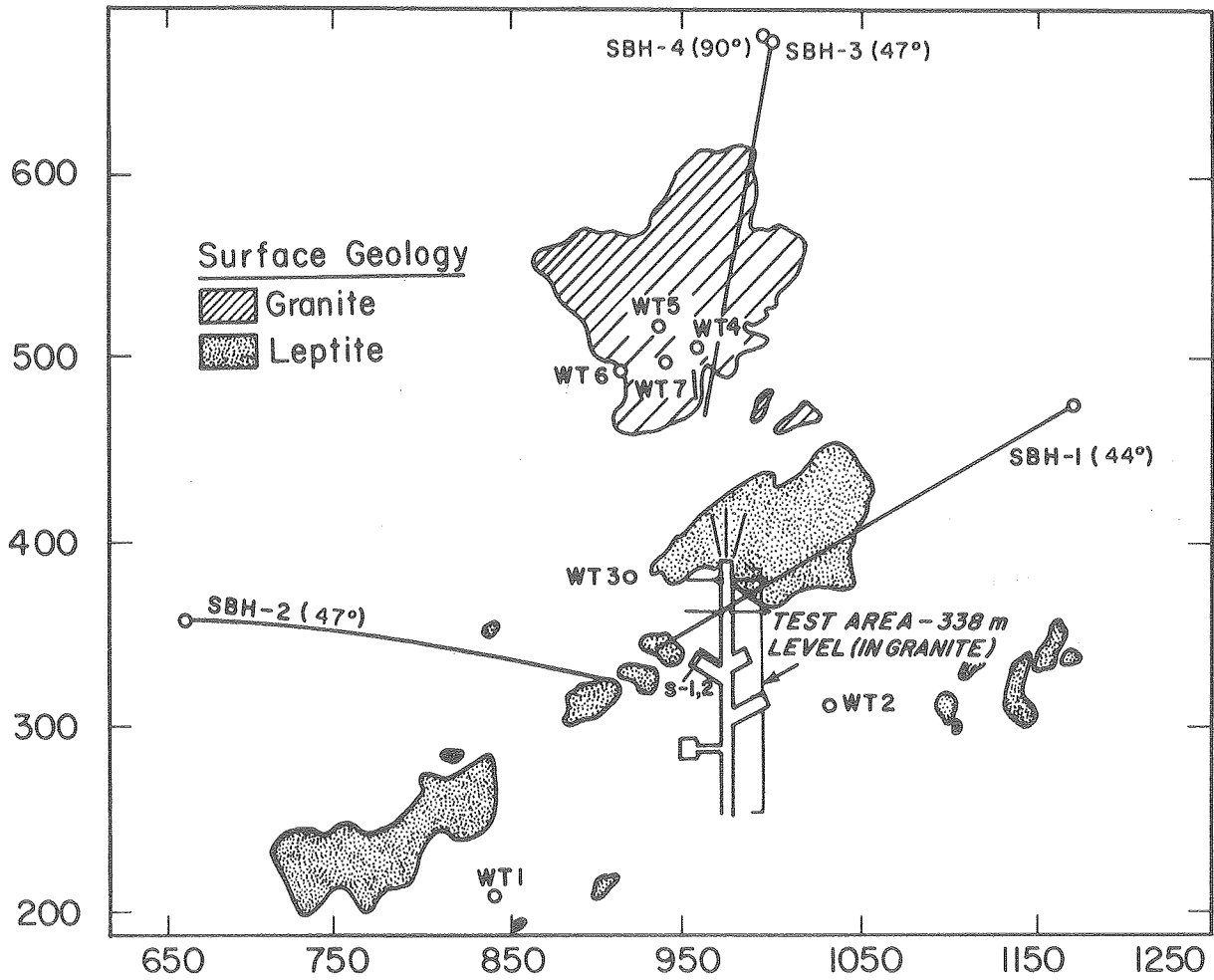
Fig. 1.   Plan map of the Stripa site in central Sweden showing rock outcrop, inclined surface boreholes and underground experimental drifts. Mine coordinates given in meters.

XBL 792-7380B

The rock is highly fractured, but the majority of the fractures are tightly healed. Common fracture-filling minerals are chlorite, sericite, quartz, epidote, and carbonate minerals, with fluorite and opaques (often pyrite or hematite) less common (Wollenberg et al., 1981).

The leptite consists of strongly metamorphosed rhyolite lavas and tuffs. Almost all of the iron ore deposits occur in the leptite. The leptite composition is similar to that of granite, except that the mafic mineral content is generally higher, especially in the iron-rich horizons where the leptite assumes a distinct banded character. Like the granite, the leptite is highly fractured. Fracture mineralogy is similar to that of the Stripa granite, but with epidote being more common in the leptite.

2. CHARACTERIZATION OF THE ROCK UNITS

A combination of geophysical measurements is an important aid for the recognition and characterization of the physical properties of different rock units along the borehole. The penetrated rock types can therefore be divided into sub-units characterized by different bulk physical properties.

Core drilling gives an almost continuous record of the penetrated rocks and therefore its compositional variations, structure, fractures and fracture coatings can be determined. The core is investigated mainly by visual inspection, with more detailed studies carried out on a few samples. Sub-units of rock types characterized by different bulk physical properties are not always observed visually. This might be due to microscopic variations, for example, texture and microfracturing. Some mineralogical variations may be detectable only by chemical analysis or microscopic investigations of thin sections. Thus, geophysical borehole investigations can give valuable complementary information about the physical properties of the rocks. This information also can be used to direct sampling of the core for geomechanical, chemical, and mineralogical investigations. Reexamination of the core in order to check for the different sub-units established by borehole geophysics often shows the slight differences in coloring, texture, and mineral distribution between units that were overlooked in the first inspection.

The physical contrast between leptite and granite is visible in several logs, but is most clearly seen in the following (Fig. 2a):

    o   gamma-gamma: the leptite is a denser rock than the granite

    o   natural gamma-ray: the leptite has a lower count rate than the
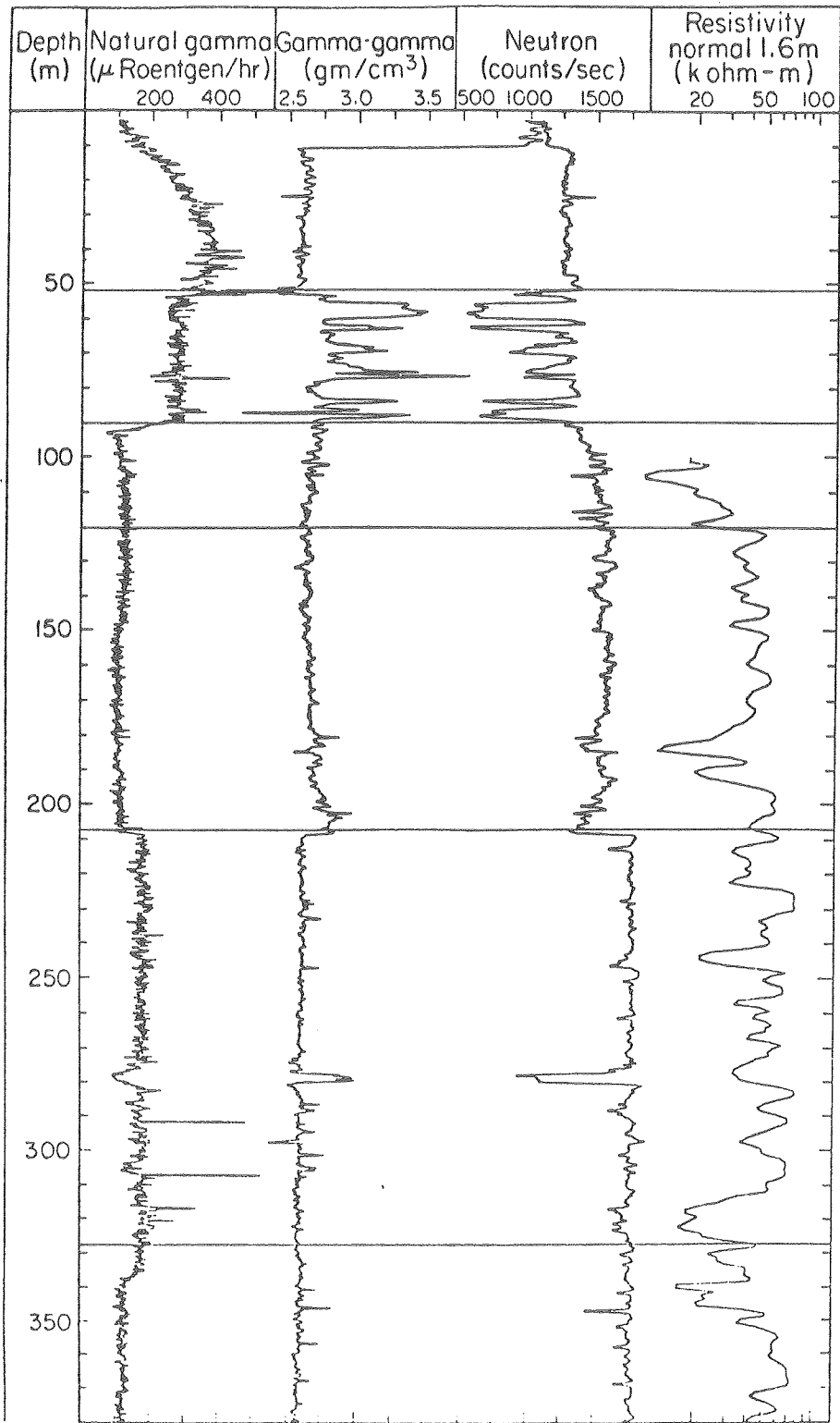
XBL 811-2545

Fig. 2a.   Geophysical logs in borehole SBH-1. Water level is at 80 to 90 m.
Much of the high gamma ray response is due to radon daughter
products within the borehole (see text).
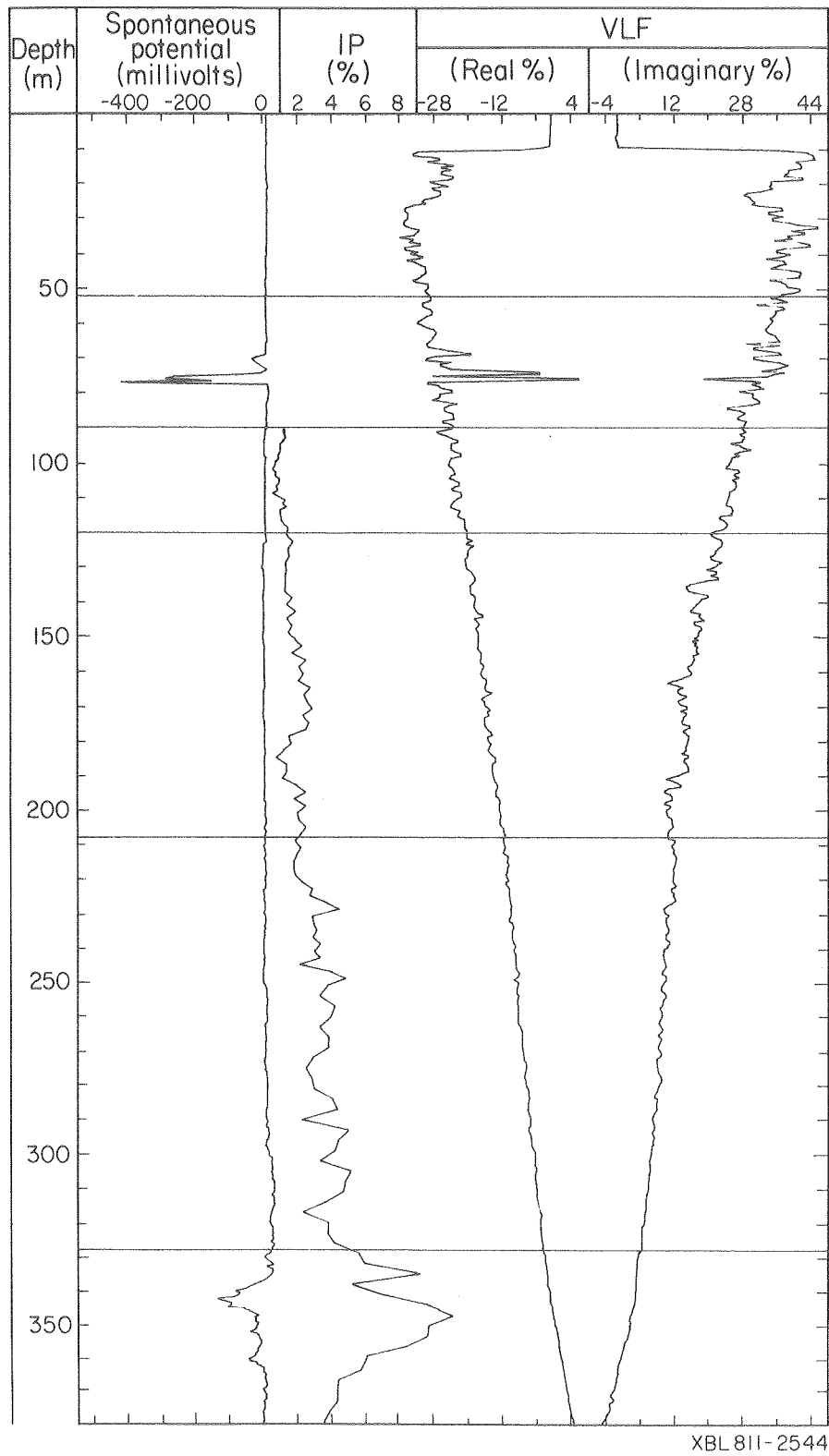
Fig. 2b.   Geophysical logs in SBH-1, as in Fig. 2a.

adjacent granite

o neutron: the leptite has a higher content of mafic minerals (see section on specific minerals) and a slightly higher porosity than the granite.

Waveform records of the leptite (not shown) are generally more disturbed, reflecting more fracturing, though at greater depth one cannot distinguish the granite from the leptite using just the acoustic waveform log. Also, the Stripa leptite unit has a lower maximum resistivity of 60,000 ohm-m compared to a maximum resistivity of 80,000 ohm-m in the granite.

The water level in the hole was at 80 m during LBL's measurements and at 90 m during SGU's measurements. The electrical measurements (point resistance, differential resistance, resistivity, IP and SP) need water-filled boreholes to enable electrical contact between the electrodes (in the tool) and the surrounding rock. However, inflowing water above the water table will flow along the lower borehole wall down to the water table. Due to the 45° inclination of the borehole there is enough water along the borehole to get reliable SP measurements (Fig. 2b).

In a comprehensive study of all the gamma-ray logs at Stripa, Nelson et al. (1980) found that extremely high concentrations of radon in groundwater have contributed to the gamma ray levels measured in boreholes wherever there is sufficient movement of water into a borehole. The uranium-238 concentration in Stripa granite is in the 30 to 40 ppm range, considerably greater than in most silicic rock, and uranium is apparently distributed in the rock such that emanation of radon into water-filled cracks and fractures is quite high. The radon is then transported by groundwater flow through fractures

into the open borehole, where gamma rays emitted by its daughter products, bismuth-214 and lead-214, are detected by the gamma probe. Gamma spectrometric measurements on core samples have determined that the uranium concentration is fairly uniform throughout the Stripa granite. Where the rock contributes all of the gamma emission, the probe measures 120 µR/hr in granite. This level is reached only at the bottom of SBH1 below 340 m in Fig. 2. Throughout the rest of the hole excessive counts are provided by radon-charged water which infiltrates into the hole above the water level, trickles down the side of the hole to the top of the water column, then continues to move downward in steady flow to about 320 m, where most of the water exits the hole at a major fracture zone. Superposed on this pattern are variations in count rate due to variations in radioelement concentration of the wall rock; the natural background of the leptite is obviously less than that of the granite.

Both the granite and the leptite are subdivided according to physical property changes apparent in the geophysical logs. These zones are described below and summarized in Fig. 3. The depth stated is the slant depth along the borehole, not the true vertical depth, which can be approximated by multiplying the slant depth by 0.7.

2.1 Upper Granite, 0 - 52 m

The striking buildup in the gamma curve is attributed to the infiltration of radon-charged water into the borehole. The maximum at 40 m indicates that most of the infiltration occurs above this depth. Caliper openings (not shown) are most frequent above 25 m. The natural gamma activity is so high

Depth (m)　　　　　Summary Descriptions

UPPER GRANITE: WATER WITH HIGH RADON CONTENT SEEPING INTO BOREHOLE.
UNIFORM GAMMA-GAMMA AND NEUTRON RECORDS WITH HIGH COUNT RATES COMPARED
WITH THE LEPTITE, INDICATING A LOWER CONTENT OF MAFIC MINERALS.

50

IRON-RICH LEPTITE: FLUCTUATING GAMMA-GAMMA AND NEUTRON COUNT RATES REFLECT
A BANDED CHARACTER WHERE SOME BANDS HAVE HIGH CONTENT OF MAFIC MINERALS. THIS
UNIT IS MORE FRACTURED THAN ANY OTHER UNIT (CORE LOG, CALIPER).

100　TRANSITIONAL LEPTITE: NO BANDED CHARACTER. DECREASING CONTENT OF MAFIC
MINERALS AND DECREASING FRACTURING WITH DEPTH (ACOUSTIC WAVE FORM).

LOWER LEPTITE (UPPER PART): MARKED DECREASE IN FRACTURING (ACOUSTIC WAVE FORM).
UNIFORM NEUTRON AND GAMMA-GAMMA RECORD INDICATING A MORE HOMOGENOUS ROCK
150　COMPARED WITH IRON-RICH AND TRANSITIONAL LEPTITES.

LOWER LEPTITE (LOWER PART): TWO SECTIONS WITH DECREASED NEUTRON AND GAMMA-
GAMMA COUNT RATES WHICH INDICATE AN INCREASED CONTENT OF MAFIC MINERALS.
CHANGE IN SLOPE OF THE VLF RECORD, INDICATING THAT THIS CHANGE IN THE
200　PROPERTIES OF LEPTITE IS NOT JUST A LOCAL PHENOMENON CLOSE TO THE BOREHOLE.

250　LOWER GRANITE: INCREASED GAMMA-RAY ACTIVITY DUE TO HIGHER RADIOELEMENT
CONCENTRATION THAN IN LEPTITE. INCREASE IN NEUTRON AND GAMMA-GAMMA COUNT
RATES, INDICATING DECREASED CONTENT OF MAFIC MINERALS. INCREASED IP EFFECT.
MAJOR FRACTURE ZONES IN THIS INTERVAL.

300

PYRITIC GRANITE: CHARACTERIZED BY PYRITE ALONG FRACTURES AND/OR IN VEINS.
A HIGH IP EFFECT INDICATES INCREASED CONTENT OF SULFIDES. THE SECTION WITH
350　THE MOST SULFIDE MINERALIZATION IS CHARACTERIZED BY A MARKED SP ANOMALY
AND LOWER RESISTIVITY. CHANGE IN THE SLOPE OF THE VLF RECORD INDICATES THAT
THIS MINERALIZATION HAS A LARGE EXTENT. FRACTURES ARE CLOSED, ACCORDING
TO SONIC LOG.

XBL 811- 2547

Fig. 3.　Summary of geological inferences based on inspection of the
geophysical logs.

in the hole that the gamma-gamma response is affected in this zone and cannot be compared with that of the lower rock units. Because the hole is air-filled in this upper zone rather than water-filled, the neutron response is shifted compared with that of granite lower in the hole; however, the response can be compared directly with that in the leptite down to the top of the water column.

2.2. Banded Leptite with Iron-Rich Zones, 52 - 89.5 m

The outstanding features in this zone are the gamma-gamma and neutron fluctuations shown in Figure 2a. As discussed further in the section on mineralization, the iron-rich intervals are clearly delineated by the reduced count rates recorded by the two logs. The caliper log (not shown) indicated that the borehole wall is rougher than any other interval in the hole, although the diametral increases are only a few millimeters. The short portion of sonic record obtained in this interval confirms that it is more fractured than any other interval in the hole. The iron-rich intervals appear to be more broken than the iron-free intervals. The constancy of the gamma count rate reflects the fact that the granite rather than the leptite is the radon source, and that no signficant dilution occurs within this interval. That is, there may be some entry of water within this interval, but it is either of insufficient volume or insufficient radon content to perturb the gamma record.

2.3 Transitional Leptite, 89.5 - 120 m

This is a transitional zone between the fractured, banded leptite above and the competent leptite below. The neutron and gamma-gamma logs are more uniform, lacking the banded character of the iron-rich unit. There is an

increase in the neutron count rate (1,340 to 1,600 counts/sec) from the contact
at 90 to 115 m, and also a less pronounced density decrease in the gamma-
gamma log attributed to a decrease in mafic mineral content. The sonic
waveform, gamma-gamma, caliper and core logs all indicate that fracturing
decreases with depth in this interval. The low uniform IP effect of 1%
indicates that sulfide and clay content is negligible.

2.4 Lower Leptite, 120-208 m

The lower leptite is a more competent and less fractured rock than
the transitional leptite unit. This change in competence is best revealed by
the acoustic waveform record (not reproduced here; see Fig. 2.4 of
Nelson et al., 1979), which is generally quite uniform throughout the 120-
208 m interval. Those anomalous zones that are present reveal individual
features of less than 1-m intercept. At a depth of about 148 m the gamma-ray
activity decreases from 120 to 100 μR/hr. This step-like decrease is attri-
buted to a decrease in the radioelement concentration in the leptite.

There are no indications in the neutron or gamma-gamma records when
passing into the lower leptite unit. However, the lower part of this unit,
170 to 208 m, does have a more variable neutron and gamma-gamma count rate.
Two sections in particular, from 177 to 188 m, and from 192 to 208 m, have
low neutron and gamma-gamma count rates (Fig. 2a), indicating higher mafic
mineral content. Also, the rock appears visually somewhat darker in these
intervals. Electrically these two intervals can be separated. The upper
one, from 177 to 188 m, is of reduced resistivity and IP response, and the
lower one, from 192 to 208 m, is of higher IP and resistivity.

The real VLF component shows a slight change in slope and the imaginary VLF component a marked change in slope at 170 m (Fig. 2b). It seems probable that the resistivity decrease and its associated compositional change is not a local phenomenon close to the borehole but has a large lateral extent.

2.5 Lower Granite, 208 - 328 m

The granite has a higher gamma count rate than the leptite, due to the higher radioelement content, and higher gamma-gamma and neutron responses due to the lower mafic mineral content. Its IP effect of 2.5 to 4.0% is somewhat higher and more variable than the leptite.

The logs show that the lower granite is more fractured than the lower leptite above and the pyritic granite below. Two 8-m fracture zone intercepts stand out at 272.5 - 280 m and at 316.5 - 324.5 m (Figs. 2 and 8). The latter is permeable enough to permit flow under steady-state open hole conditions, as shown by the gamma ray and temperature logs.

2.6. Pyritic Granite, 328 - 380 m

The pyritic granite unit is characterized by fractures containing sulfides, mainly pyrite, which are rare in the other units. A most pronounced difference between the lower and pyritic granites is the very marked SP and IP anomalies indicating rather extensive sulfide occurrences. The peaks of the SP and IP anomalies at 340 m slant depth (Fig. 2b) coincide with the section of highest pyrite content. Both components of the VLF record show a change in slope when passing into the pyritic granite. Thus the sulfide occurrences are not just isolated occurrences close to the borehole but must have considerable extent.

A second distinction between the two granite units is provided by the sonic log. At 328 m there is a noticable decrease in the frequency of sonic waveform features; in fact, below 338 m the sonic waveform record (see Fig. 8 in Section 5) is remarkably free of any anomalous features. Here, the core log is not consistent with the sonic record in that the frequency of observed fractures in core does not decrease below 328 m. At 337 m the gamma-ray log drops 40%. The decline is due to loss of radon-charged groundwater from the borehole into a permeable fracture. With this notable exception, the logs give no evidence of significant fracturing within the pyritic granite.

3. EFFECTS OF SPECIFIC MINERALS

The mineralogical variations seen in the core have characteristic responses on some of the geophysical logs. The occurrence of quartz veins, pegmatite dikes, sulfides, mafic minerals, and iron oxides can be identified in igneous and metamorphic rocks by using a combination of geophysical borehole logs. Such identification is in fact necessary so that their effects can be eliminated or avoided in analyzing the logs for fluid flow properties.

3.1 Iron Oxides and Silicates

Examination of the gamma-gamma and neutron logs in Fig. 1 and in the expanded log section in Fig. 4 shows a number of well-defined concident deflections. Spike-like decreases in the gamma-gamma count rate caused by density increases are often associated with decreases in the neutron count rate, which would usually be attributed to increasing water content. However, porosity effects cannot produce such coincident responses, because a bulk density increase without a grain density increase implies a porosity decrease, not an increase. The effect of bound water is more difficult to assess here, since in some cases mineralogically bound water can completely dominate the neutron log (Nelson and Glenn, 1975). It may well be a contributing factor to the neutron response in SBH-1, but it is not believed to be the controlling factor because some of the observed deflections are too large to be accounted for by bound water. Borehole roughness is also discounted because the caliper shows that diametral roughness is usually less than a few millimeters, not enough to affect the neutron log, and opposite in effect to the observed density increases. We therefore attribute the density increases
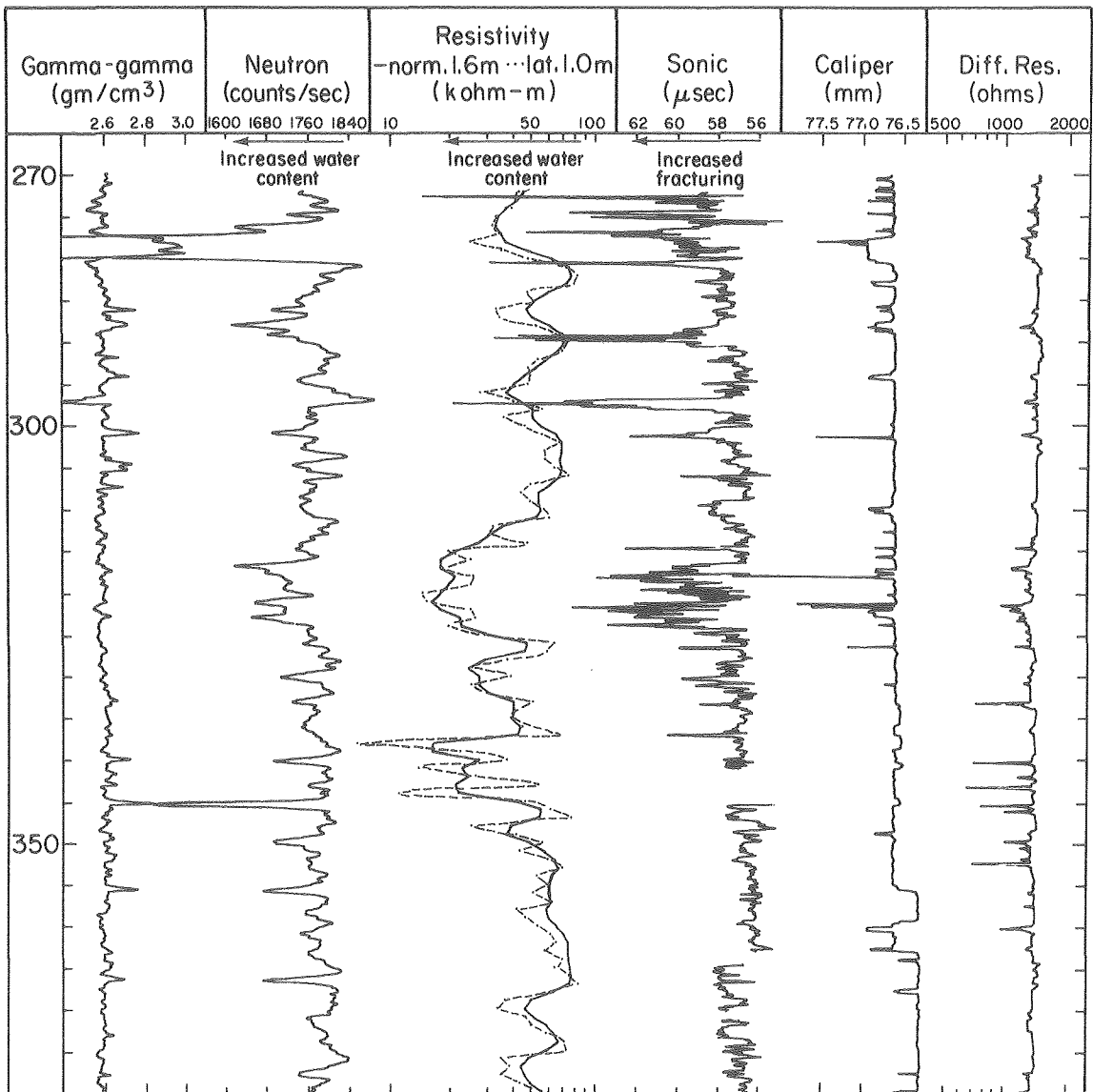
Fig. 4.   Geophysical logs in SBH-1, section 270 to 380 m.   The sumbol py denotes presence of pyrite in core.

to the presence of dense minerals, the chief heavy constituent being iron. Iron is also a good absorber of thermal neutrons, having an absorption cross-section about 15 times greater than that of silicon.

The core record shows that iron is usually visually present wherever the anomalous deflections occur. Pyrite and chlorite are present in the interval 337 - 345 m where three such anomalous peaks are located. Two greenstone intercepts, at 245 - 246 m and 277 - 280 m, coincide with two similar neutron and gamma-gamma deflections. The effect is most dramatic in the banded leptite unit from 52 to 89 m, where the leptite consists of bands of very fine-grained, light-gray rock alternating with bands of mottled green coloration. The neutron and gamma-gamma deflections of Fig. 2a match perfectly with the green zones, which are generally about one meter thick. On the basis of thin section inspection, the rock at 87.9 m depth is composed mostly (~80%) of an iron-rich amphibole, probably actinolite, intergrown with epidote, which comprises 10 to 15% of the sample. A thin section from 86.5 m shows the rock to be a breccia comprised mostly (~90%) of chlorite and epidote, with interstitial fine clay. In addition, the high-density, high-absorption records at 76 - 77 m correlate well with iron oxides, probably hematite, observed in core. These observations clearly document the high percentages of iron-rich minerals hematite, epidote, chlorite, and actinolite within the 52 to 89 m depth interval.

A fraction of the coincident gamma-gamma and neutron peaks, selected to omit fractured intervals, are cross-plotted in Fig. 5. Two trendlines represent least-squares fits through the points from the granite and leptite intervals which lie below the water level. The range of points from the
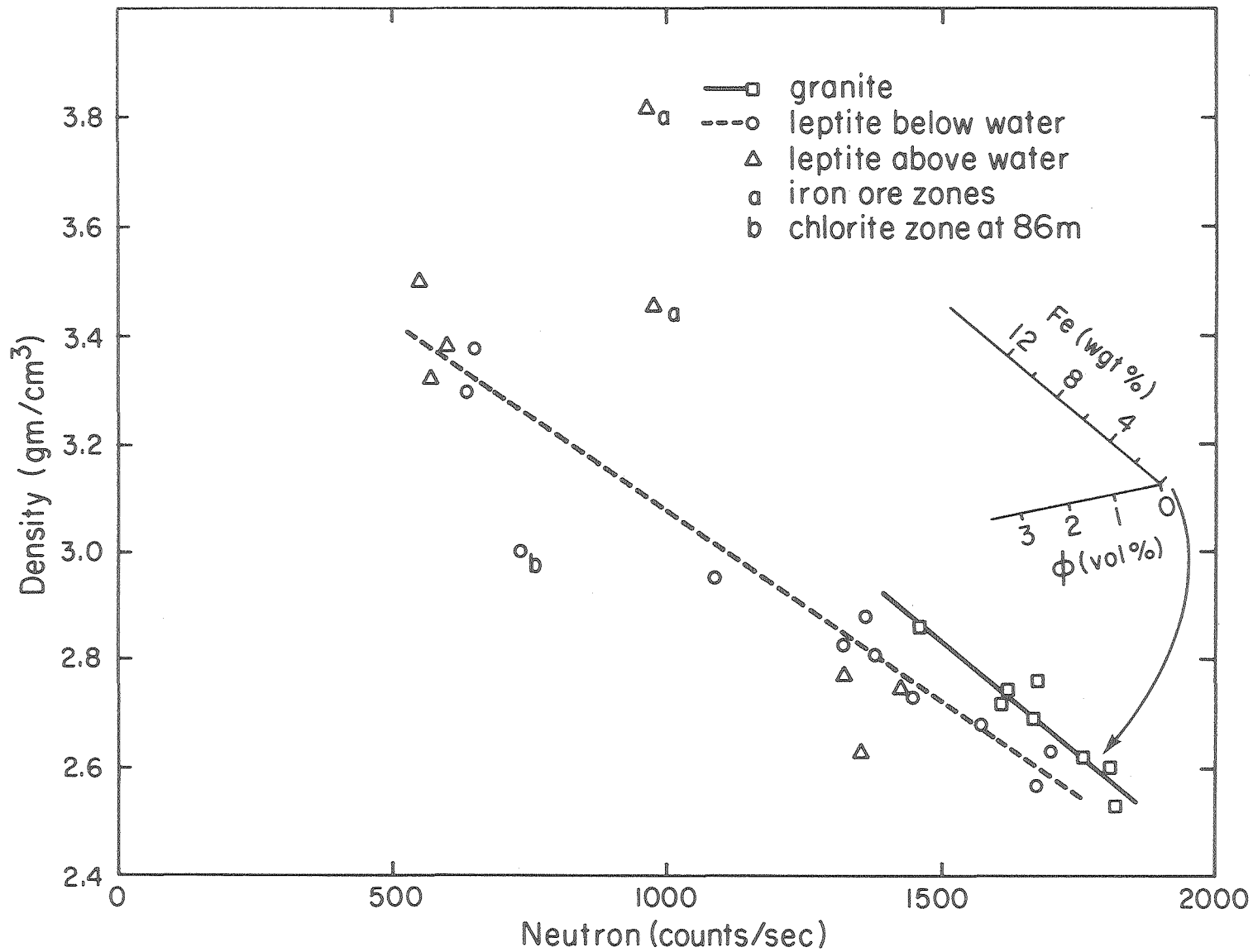
Fig. 5.   Density anomalies from the gamma-gamma probe plotted against
          correspnding neutron respnses. The overall trend is dominated
          by iron-rich minerals rather than the water contained in fractures
          and pores.

XBL 811-2543

leptite is much greater than the granite samples, since the iron content of the leptite varies much more widely. Despite this, the two straight-line fits are nearly parallel, indicating that the gamma and neutron absorption mechanisms are similar in the two rock types. Inserted into Fig. 5 is an approximated scale reflecting the effect of porosity and iron variations, which are expressed as

$$N(cps) = 1800 - 85\varphi - 24 \text{ Fe},$$

and

$$\rho_b(gm/cc) = (1 - 0.01\varphi)(2.62 + 0.02 \text{ Fe}) + 0.01\varphi \quad ,$$

where N is neutron count rate, ρ_b is bulk density, φ is volume percent porosity and Fe is weight percent iron. The porosity scale, based upon the above expressions for zero Fe content, explains the offset between granite and leptite trends as due to the leptite having a porosity about 1% higher than the granite. The Fe scale was established by computing the bulk density for increasing amounts of iron substituting for magnesium in chlorite [composition: $(Mg, Fe)_6 Si_4O_{10}(OH)_8$], and adhering to the trendline established empirically for the granite. Hence it should be recognized that these scales are appropriate only for this particular neutron probe, and are probably valid only over small excursions of iron and porosity from the chosen base values.

3.2. Pyrite

As mentioned before, the granite at the bottom of the borehole (328 - 380 m) contains sulfide minerals. Pyrite constitutes less than 1% of the minerals seen in core, except in the interval 338 - 345 m, where it occurs more abundantly, filling fractures or in veins along with quartz and chlor-

ite. These sulfide-mineralized sections of core typically contain 2 - 10% pyrite and are 6 to 30 cm in width.

Within the interval 330 - 355 m (Fig. 4), the pyritic zones are reflected in peaks on the gama-gamma, neutron, resistivity, and resistance logs. The neutron and gamma-gamma peaks are believed to be controlled by the iron content, while the electrical logs respond to the enhanced conductivity.

Over this same interval, the IP log (Fig. 2b) increases to over 8%. Because the IP log was run on a 5 m electrode spacing, it lacks the spatial resolution of the other logs already mentioned; however the broad peak convincingly demonstrates the existence of sulfides. At other depths in the hole, the IP response declines where the resistivity drops (compare 245 m and 317 m, for example); that is, above 330 m much of the IP response is controlled by porosity fluctuations. However, below 330 m the IP and resistivity logs no longer correlate, and the IP response is dominated by the sulfide content.

The spontaneous potential (SP) log, also shown in Fig. 2, responds within the pyritic interval as does the IP log. Note that the SP log is featureless throughout the hole except at the iron sulfide and iron oxide mineralization occurrences. The series of pyrite occurrences is extensive enough to produce a clear change in the gradient of the VLF records.

4. POROSITY AND WATER CONTENT

Four of the probes run in SBH-1 respond in some way to the volume fraction of water-filled pore space. Each of these, the gamma-gamma, neutron, electrical resistivity, and sonic probes, has been used to a greater or lesser extent to estimate porosity in sedimentary reservoir rocks. In igneous rock of low porosity it is not at all obvious that a particular technique has adequate sensitivity to measure small porosity variations, or that other competing factors will not mask the porosity effect.

One of these four, the gamma-gamma probe, lacked the sensitivity required to measure porosity fluctuations at the 0.01 level. Calibration of this particular probe (see Appendix), along with count rate and averaging time considerations, shows that density variations less than 0.06 gm/cm^3 are not detectable. If the grain density ρ_g is held constant at 2.65 gm/cm^3, then an apparent change in bulk density ρ_b affects the porosity as

$$\Delta\psi = -\Delta\rho_b/(\rho_g-1) = -0.6 \ \Delta\rho_b \quad .$$

Consequently the gamma-gamma probe is insensitive to fractional porosity changes less than 0.035. Visual inspection of the log in Figs. 1 and 4 shows that the gamma-gamma probe responds well to variations in mafic mineral content. However, aside from these variations in grain density, the gamma-gamma record is uniform and shows no influence from fracture zones or any other significant porosity-controlled density decreases. It appears that porosity increases of more than 0.035 are uncommon in SBH-1, an observation corroborated by the neutron and resistivity logs discussed in the following paragraphs.

On the other hand, the neutron, resistivity and sonic records indicate a number of porosity increases of less than 0.035, most of which occur at fracture zones. Lacking core measurements of the actual porosity (which are not meaningful in fractured media), a standard method of examining physical effects on pairs of logs is to use cross plots (Figs. 6 and 7). Values of correlated features are digitized and plotted, without any correction applied to the neutron and sonic logs, but with borehole and Archie's law considerations incorporated into the resistivity evaluation. Mafic zones identified by the gamma-gamma log are generally excluded from the cross-plots.

As discussed in the Appendix, the neutron probe was calibrated in a granitic block, giving the dependence of neutron count rate N upon porosity ϕ

$$N = C - D\phi \quad ,$$

where C and D are constants for a given rock type. The D values of -85 cps per one volume percent is assumed to hold approximately for the Stripa granite. The C value, more subject to matrix effects, is fixed somewhat arbitrarily in Fig. 6 to give reasonable porosity values based on water content of the calibration block.

The electrical resistivity data are reduced to formation factor, $F = R_t/R_w$, where R_t is the true formation resistivity and R_w is the effectiveresistivity of the pore fluid. Due to the high resistivity contrast between the borehole fluid and surrounding rock, the current density is higher in the fluid and in the rock close to the borehole. To account for this loss of spherical symmetry, the formation factor F is determined from a borehole correction chart such as Fig. 22 in Glenn and Nelson (1979), by
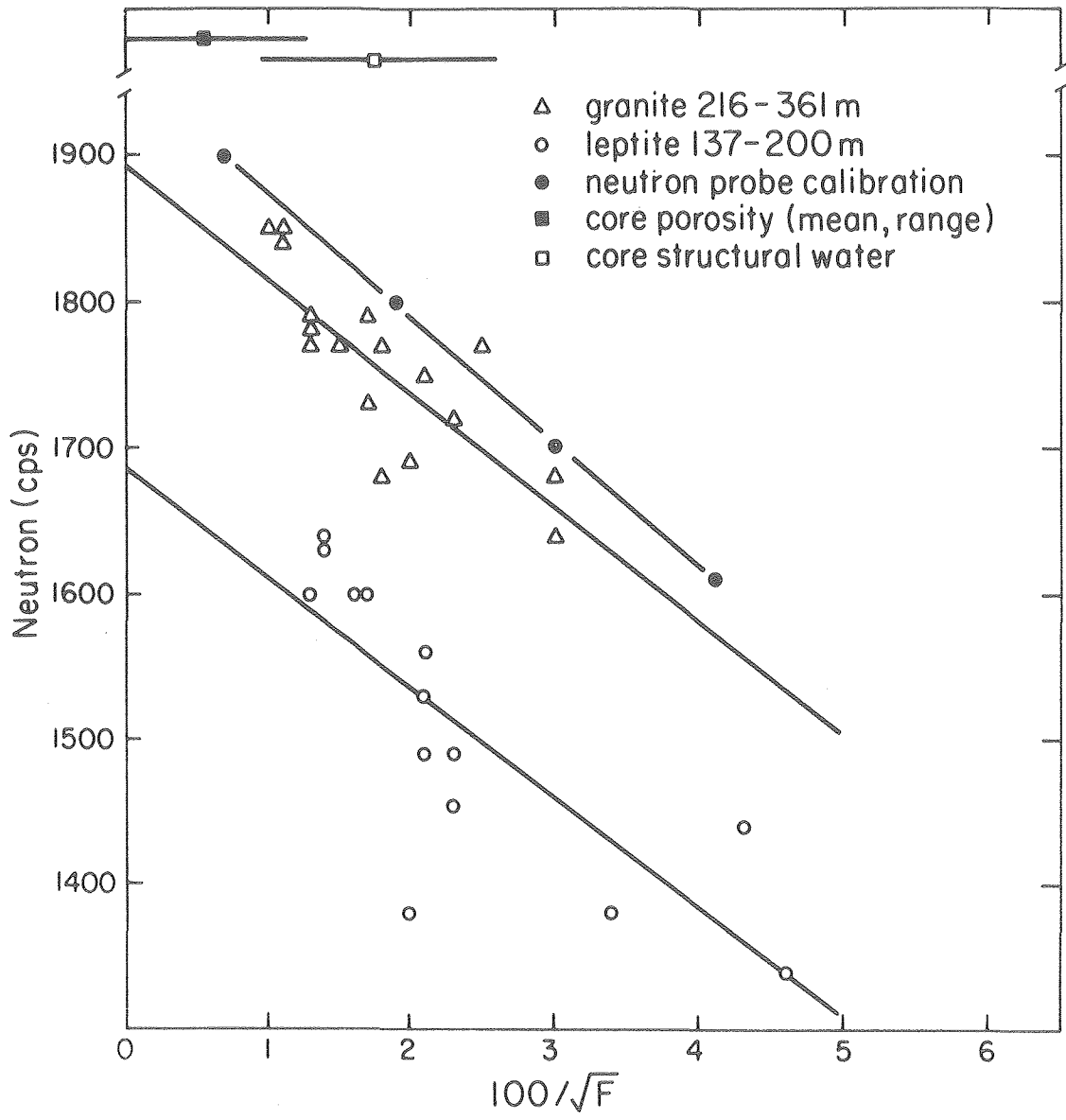
XBL 811-2542

Fig. 6.   Neutron-resistivity cross-plot for SBH-1. Conversion of apparent
resistivity values to formation factor F is described in the text.
Bottom scale is equivalent to volume percent porosity. Standard
deviation of neutron count rate is equivalent to the size of the
symbols. Straight lines represent least-squares fits to the
probe calibration, the granite data, and the leptite data. Mean
values and range of core porosity and structural water measurements
are given at top of figure.
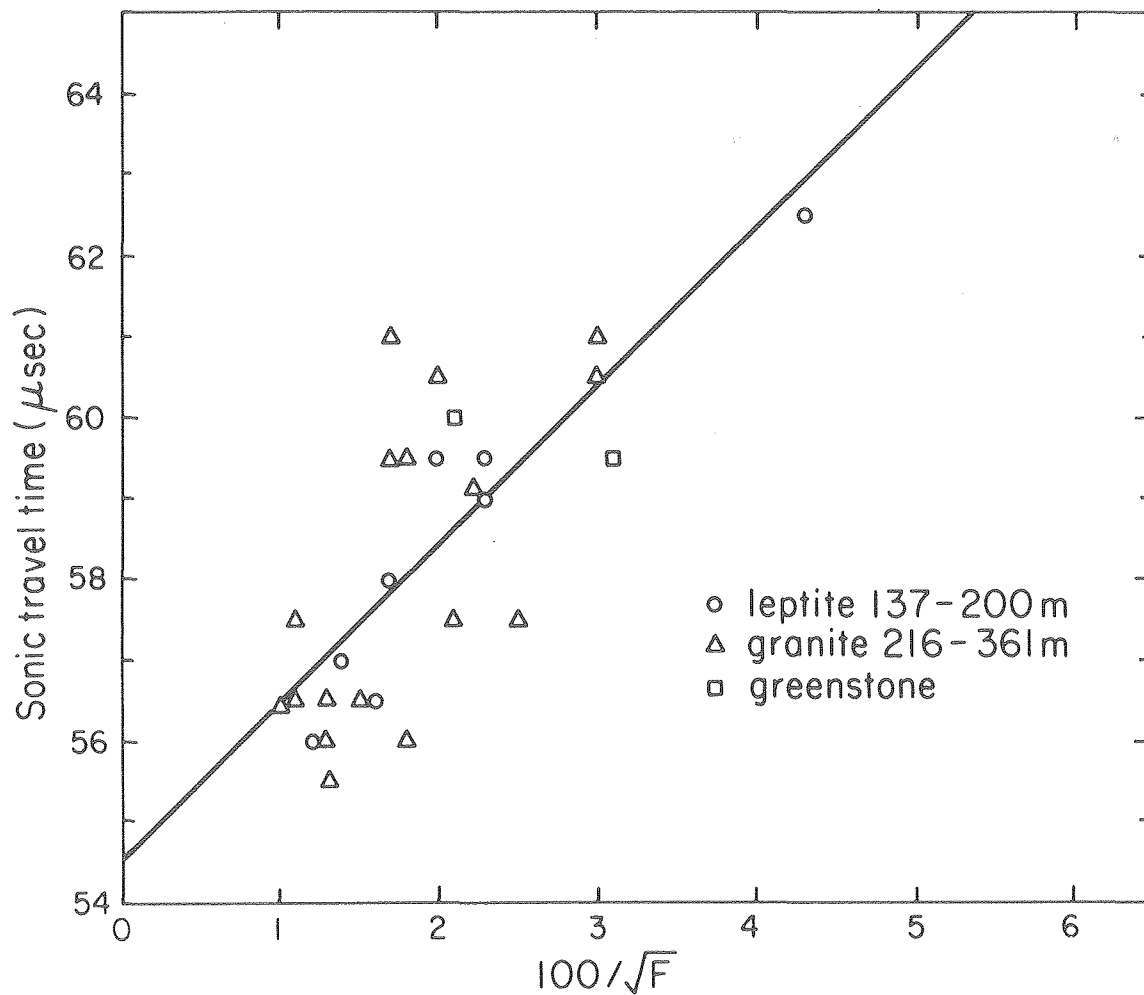
Fig. 7. Sonic-resistivity cross-plot for SBH-1; resistivity conversions are same as in Fig. 6. Data from all three rock types are included in the least-squares fit. Sonic travel times are uncompensated for probe effects.

entering the ratio of measured (apparent) resistivity R_a to fluid resistivity R_w, and the ratio of the 1.6 m electrode spacing to the 76 mm borehole diameter. For this particular data set, the non-linear chart correction yields R_t values roughly equal to 0.6 R_a. No bed correction was applied; that is, the effect of adjacent rock units of different resistivity was ignored.

The reciprocal square root of F is plotted in Fig. 6 to give a porosity estimate according to Archie's law,

$$F = \varphi^{-m} \quad ,$$

where m appears to be about 2.0 for igneous rock (Brace and Orange, 1968). The horizontal scale of Fig. 6 is therefore equivalent to volume percent porosity; some laboratory measurements on granite core samples taken from an underground borehole near the bottom of SBH-1 are included in Fig. 6 to show the water content of relatively unfractured rock.

The evaluation of R_w presents two problems. Measurements of underground waters at Stripa (see appendix of Fritz et al., 1979) range between 38 and 50 ohm-meters. However, fluid resistivity in parts of the borehole could be either higher or lower due to infiltration during and after drilling, so the uncertainty is even greater. A more serious problem is that surface conduction effects can significantly reduce the effective pore water resistivity below that of the bulk sample. Such effects can be compensated for in some sedimentary situations (Waxman and Smits, 1968). Brace et al. (1965) found that in igneous rock, the correction for surface conduction can be as much as a factor of 10, but no means of applying such a correction has yet been developed.

Faced with the dual problem of inadequate measurement and no compensation for surface conduction, we have chosen to let R_W vary as an independent parameter, successively iterating to remove borehole effects until the least-squares slope approximately matches the calibration slope for the neutron probe. This procedure is permissible because surface conduction and electrolyte conduction contribute additively to the overall conductivity, as demonstrated experimentally for a suite of low-porosity rock samples by Brace et al. (1965), and for clay-rich sandstones by Waxman and Smits (1968). Because of the two-element additive conductivity model, an equivalent water resistivity equal to $R_W R_S/(R_W + R_S)$ can be allowed to vary independently to achieve the fit without knowledge of R_S, the surface resistivity contribution.

The resulting data values using a 9.0 ohm-meter R_W are shown in Fig. 6. The 9.0 ohm-meter estimate is only as realistic as the other assumptions implicit in Fig. 6, such as the validity of the neutron calibration, its applicability to Stripa granite, and the correlation of adjacent peaks on the neutron and resistivity logs. Also, the neutron response may be distorted because fracture zones are generally characterized by fractures coated with hydrated minerals such as chlorite. Despite these uncertainties, the construction of Fig. 6 leaves little doubt that surface conduction must be considered in an Archies-law porosity evaluation of the Stripa granite.

The reduced counting rate of the neutron probe in the leptite separates the leptite data from the granite in Fig. 6; hence the two rock types are easily distinguished on this crossplot. Using the R_W value of 9.0 ohm-meters the leptite data also give a neutron slope of about -80 cps per

percent porosity similar to the granite, thereby indicating that the slope is not much affected by matrix effects and confirming one of our assumptions in the construction of Fig. 6. The statistics in both granite and leptite are only fair; both linear regression fits have correlation coefficients of -0.8.

The compressional wave travel times are plotted against the resistivity values in Fig. 7. The resistivity values are the same as in Fig. 6. The travel time values are taken directly from corresponding anomalous points on the sonic log; no correction has been applied for fluid travel time or for any other effects occurring over the one-foot travel path between transmitter and receiver. The least-squares line is fit to all data points irrespective of rock type. There is a suggestion that two different trend lines might be fit to the leptite and granite, but the data do not warrant separate treatment.

Figure 7 shows that transit times increase with decreasing resistivity, here expressed as an equivalent porosity. In sedimentary rock with inter-granular porosity, a cross-plot of this type would be expected to produce a linear trend because of the tendency of sonic travel time data to obey the time-average equation. No equivalent experience exists in igneous rock; in the following section we show that the compressional wave transit time is quite useful as a fracture indicator. The transit time delays must be controlled by such details of fracture surfaces as the point-to-point contact and infilling mineralogy. It seems likely that the apparent correlation of Fig. 7 will vary considerably from site to site, depending upon the details of porosity associated with fracture zones, development of alteration

products and the magnitude and direction of tectonic stress.

Norton and Knapp (1977) propose that total porosity in fractured rock be considered as the sum of the effective flow porosity ϕ_f, or that portion of the rock which constitutes permeability; the diffusion porosity ϕ_d, representing pores which are interconnected but in which flow is unimportant and chemical transport occurs by diffusion; and the residual porosity ϕ_r, which includes all pores independent of ϕ_f or ϕ_d. By considering permeability measurements and field estimates of fracture spacing and aperture, they conclude that flow porosity ϕ_f is a very small fraction of the total porosity in representative igneous rock. By conducting diffusional measurements on rock wafers in the laboratory they likewise show that the diffusional porosity ϕ_d is but a small fraction of the total porosity. The resulting inference is that residual porosity ϕ_r constitutes most (90%) of total rock porosity.

Because the different borehole probes respond to different physical properties, some inferences can be drawn from the log behavior regarding the nature of porosity structure. The neutron log is the only one of the three considered in Figs. 6 and 7 which can be considered a total porosity log; thermalization of neutrons by water occurs regardless of whether or not the pore space is interconnected. The electrical resistivity on the other hand, must be governed by the flow porosity, and to a lesser extent, by the diffusional porosity. The residual porosity and that fraction of the diffusional porosity which is discontinuous cannot contribute to electrical conduction processes. For these reasons, the correlation between the resistivity and neutron logs shown in Fig. 6 indicate that in the fractured zones the poro-

sity increase occurs totally within the flow and diffusional modes. Residual porosity is not increasing significantly or the correlation would not hold. It also seems unlikely that much of the new pore space is created by interconnecting what was residual pore space before fracturing occurred, for if this were true the neutron response would be the same in fractured and unfractured zones. It seems most likely that porosity increases associated with fracturing are of the flow/diffusional type. Since the increases are of a few volume percent, we infer that fracturing induces flow/diffusional porosity which is greater than the residual porosity and thus comprises the greater fraction of total porosity.

5. FRACTURE DETECTION

The acoustic, caliper, and differential resistance logs have the best vertical resolution of the suite of logs applied at Stripa. These logs, useful in detecting thin structures such as individual fractures and thin fracture zones, are shown in Fig. 8, together with core information. The open fractures observed in core have been averaged over 0.3 m to coincide with the transmitter-receiver separation of the acoustic probe. Fractures judged to have been not open in situ, as indicated by the lack of alteration minerals on the fracture surface, have been omitted from the fracture column. To accommodate the acoustic waveform record, the depth scale in Fig. 8a is expanded compared with previous figures.

The caliper and differential resistance respond to borehole roughness and are closely correlated (Figs. 4 and 8). Most of the caliper variations are close to its limit of resolution of 0.2 mm, as evidenced by the step-like nature of the log. Narrow spikes occur where the borehole has intercepted a fracture, causing loss of small chips from the borewall. Borehole roughness can be due to causes other than fractures, however. The broad increases in hole diameter at 360.1m, 368.8 m and 380 m coincide with the commencement of drilling after a core run, suggesting that renewed drilling sometimes enlarges the hole slightly. Operation of a mechanical caliper at this sensitivity level is unusual, but proved relatively straightforward and worthwhile in providing correlative information with the other logs.

The differential resistance is also quite sensitive to changes in borehole diameter, being at least comparable to the caliper. Laboratory tests showed that the probe is able to detect fractures of 1 mm aperture and
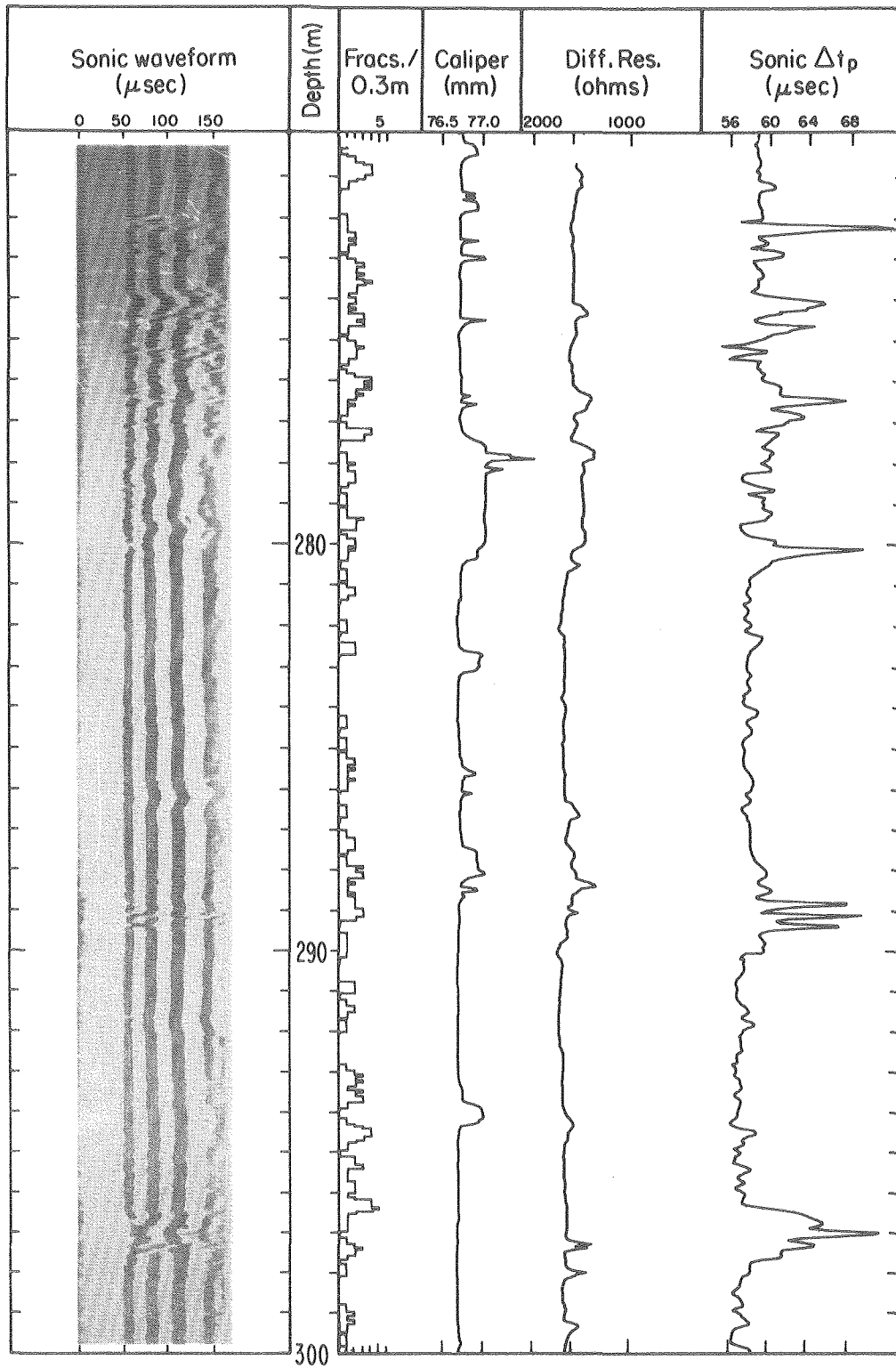
Fig. 8a

XBB811-806

Fig. 8a-d. Geophysical logs most sensitive to fracturing in granite on SBH-1.
Depth scale has been expanded to accommodate the sonic waveform
log. Core data are averaged over 0.3 m length to match the trans-
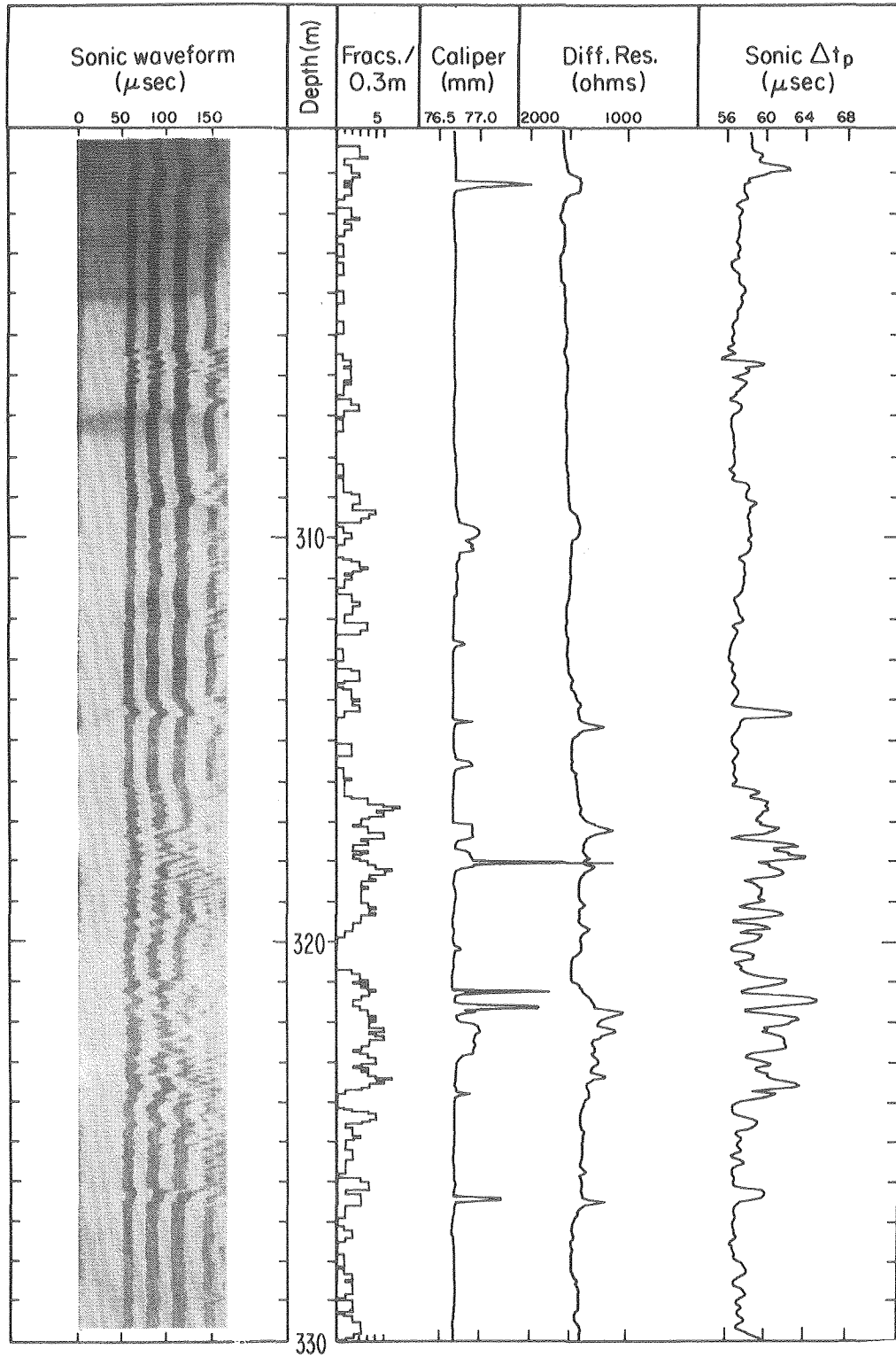mitter-receiver separation of the sonic probe.

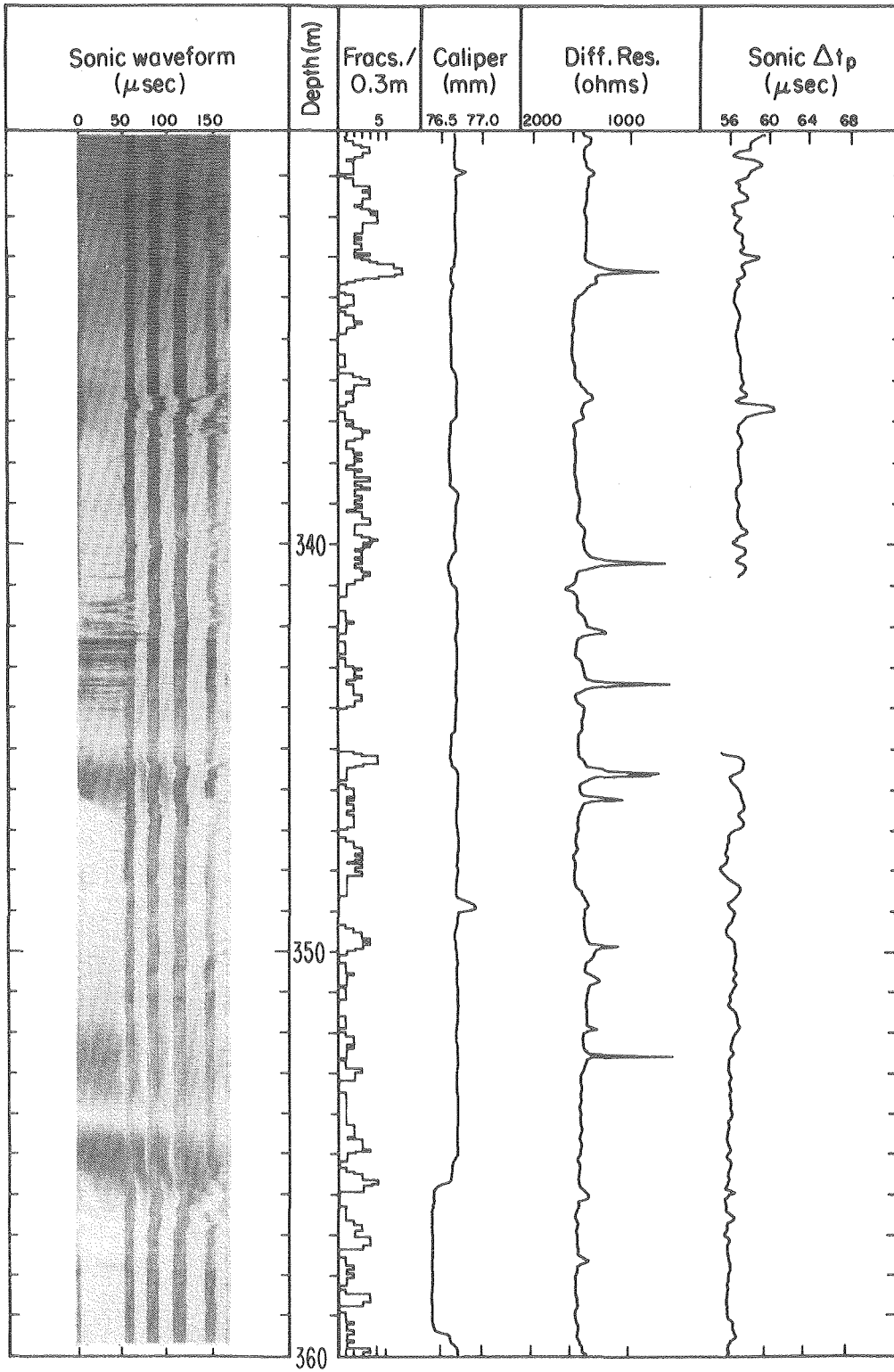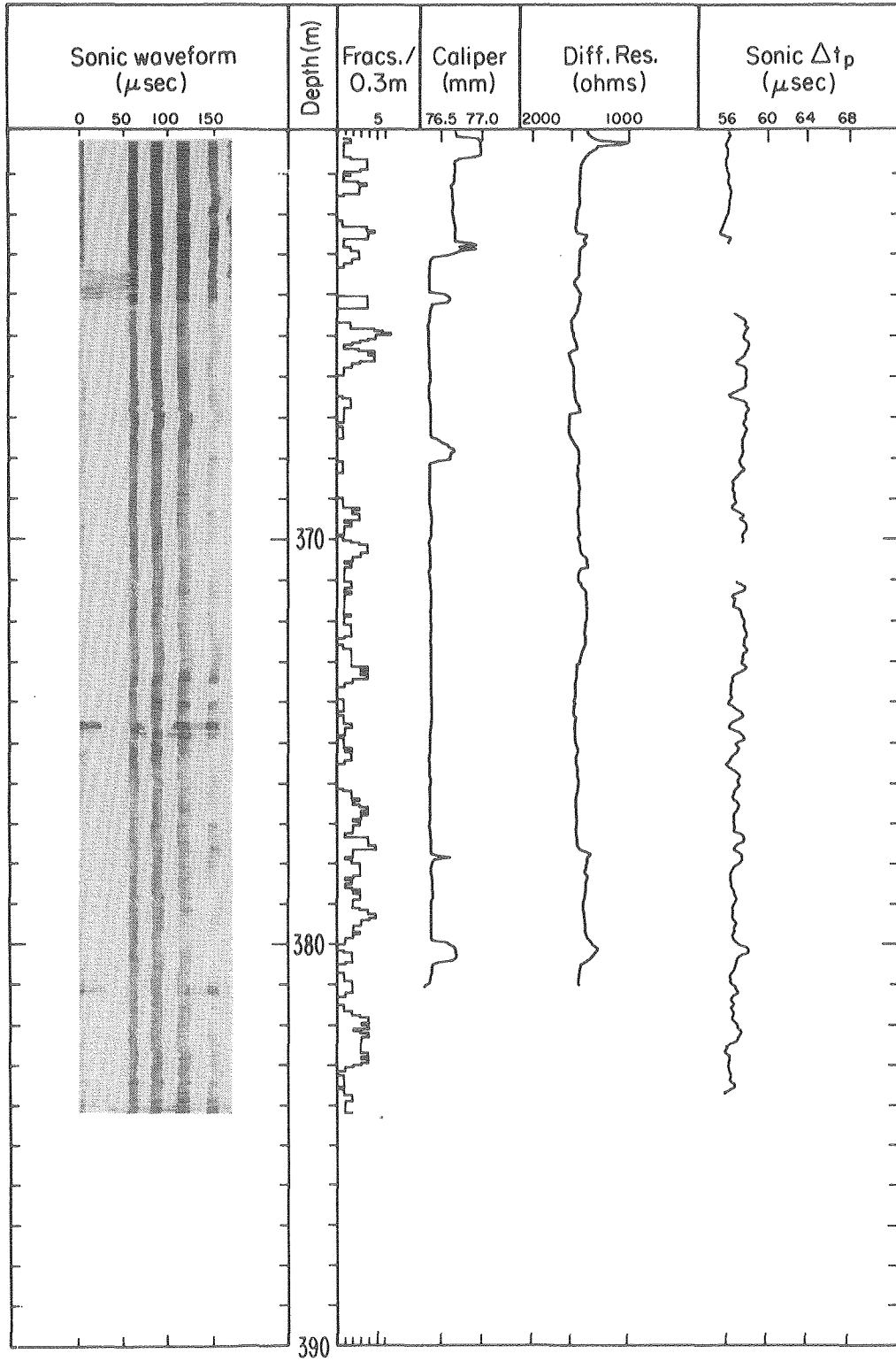-33-

Fig. 8b

XBB811-805

Fig. 8c

XBB811-804

Fig. 8d

XBB811-807

1 mm diametral depth. Its sensitivity to fracture openings which do not produce borehole roughness is not known. However, conductive veins do produce peaks in the differential resistance log, as shown in the interval between 330 m and 355 m, where pyrite is observed in core. Such mineralization shunts the current flow between the two closely spaced electrodes. Using other logs such as caliper and acoustic, which do not respond to the pyrite veins, and SP and IP, which do respond, the effect of conductive minerals can be separated from the response of open fractures.

As shown in Fig. 8, the acoustic log recordings in SBH-1 were limited to the compressional wave transit time and the waveform record on photographic film. The absolute transit time values give velocities of 5,800 m/s, comparable to those observed elsewhere on Stripa granite, both in situ and laboratory (Paulsson and King, 1980). The waveform record gives a visual presentation of zero-crossing delays and interference patterns of several wave modes. No amplitude measurements were made, although it would have been advantageous to do so. Despite these limitations, the acoustic records are the most valuable for fracture detection.

The most outstanding features in Fig. 8 are the two 8-m zones at 272 – 280 m and 316 – 325 m, where the acoustic records, caliper, and differential resistance all indicate that the borewall is disturbed and that the intervals are fractured. Open fractures in core are also more numerous in these intervals, especially in the lower of the two. In addition, the gamma ray log, already mentioned, and a temperature log (not shown) showed that the lower zone at 316 – 325 m was taking fluid even under static open hole conditions, thereby confirming the fracture logs of Fig. 8. Zones such

as these are obvious candidates for extensive hydrological testing in a
site characterization program for a waste repository. The acoustic log also
pinpoints a few other narrower zones, such as the ones at 289 m, 297m, and
337 m where fracturing is apparent.

Below 330 m slant depth, the acoustic log in particular reveals remark-
ably few fracture zones. The core record, however, continues unabated with
about the same density of open fractures to the bottom of the hole. Stress
conditions and fracture character may be such that acoustic transmission
properties change considerably below 330 m. As stated earlier, the Stripa
granite and the leptite contain numerous fractures, the majority of which are
healed. Open fractures in core are most commonly coated with chlorite,
sericite, and calcite, singly or in combination. These minerals are me-
chanically weak, so there is a good probability that fractures seen in core
were opened by the drilling and core recovery process. Analysis of the core
data from the underground experiment at Stripa by Paulsson et al. (1981)
suggests that drilling opened a large number of the open fractures seen in
the core. A comparison of TV logs with core retrieved from two 12-m holes
in the underground experiment area revealed that less than 10% of the frac-
tures open in core also appeared to be open in situ. In any case, the sonic
probe as well as the caliper and differential resistance probes appear to
provide information on fracturing in situ that the core log does not.

The compressional wave transit time has been examined by others as a
measure of fracture frequency. King et al. (1978) found in borehole mea-
surements carried out under low lithostatic stress conditions that the ratio

$(V_f/V_1)^2$, where V_f and V_1 are respectively the in situ and intact rock velocities, decreases linearly with increasing fracture frequency. A comprehensive set of refraction measurements on igneous and metamorphic outcrops were compared with fracture frequency intercepted by shallow slant boreholes in a paper by Sjogren et al. (1979). The results, averaged from 15 sites, appear to obey a dependence similar to that observed by King et al. These findings are not at all unreasonable for near-surface measurements, where a fracture observed in core is also likely to be sufficiently open in the rock mass to delay the acoustic wave. However, at depth the connection between fracture frequency observed in core and the propagation of acoustic energy will be less straightforward. Higher stress may close, partially or totally, otherwise open fractures. As noted above, many open fractures seen in the core at Stripa may be drilling induced.

The compressional wave transit time is the easiest measurement to extract from an acoustic probe, but it is not as sensitive to fractures as is the amplitude of other modes of wave propagation. For example, Dzeban (1970) simulated fractures with cuts in aluminum blocks which were then pressured to simulate lithostatic pressure. Fractures at a simulated depth of 1000 m had a significant impact on shear wave attenuation, whereas compressional waves reacted weakly to them. A recent study of acoustic borehole records by Paillet (1980) convincingly demonstrates the utility of shear and tube wave amplitude measurements for fracture detection through the correlation of gated amplitudes with fractures recorded in core and by the acoustic televiewer. In addition, Paillet's computed borehole acoustic waveforms provide additional insight into the patterns produced by interfering modes.

6. SUMMARY AND CONCLUSIONS

In characterizing prospective sites for repositories of radioactive waste, borehole logs have four purposes: (1) characterizing rock units by bulk physical properties; (2) detecting mineralogical variations; (3) monitoring differences in porosity and water content; and (4) detecting fractures. We have illustrated these applications by discussing logs from a single borehole at an experimental site at Stripa, Sweden. The following paragraphs highlight some of our specific findings on log behavior in an igneous/metamorphic rock mass.

Rock Characterization. To characterize rock units that would otherwise pass unnoticed in visual inspection of the core, geophysical logs can be used, as demonstrated in the discussion of Figs. 2 and 3. As summarized in Fig. 3, the leptite intercept can be divided into three parts: an iron-rich unit revealed by gamma-gamma and neutron responses, which is also more fractured and broken than other intervals in the borehole; a transitional unit in which fracturing decreases with depth; and a lower, competent leptite unit. The granite has two units: one where several extensive fracture zones occur within the interval 208 - 328 m, designated the lower granite; and another, below this depth, called pyritic granite, where fracturing decreases markedly and sulfide occurrences are the most outstanding characteristic.

Mineralogic Analysis. Mafic minerals produce well-defined coincident deflections on the gamma-gamma and neturon logs, due to density increases and thermal neutron adsorption. These deflections are particularly outstanding at the iron-rich zones in the leptite. The overall trend is summarized in Fig. 5. Pyrite similarly affects the gamma-gamma and neutron logs, as well as the electrical resistivity, resistance, and IP logs.

Porosity. Quantifying porosity fluctuations at the one percent level in igneous rock offers a substantial challenge for borehole measurements, especially since the nature of the pore space and its interconnectivity is not well understood. Our efforts, shown in Figs. 5 and 6, indicate that the now-standard methods used in sedimentary sequences may be applicable in igneous rock with proper modifications. For example, it is clear that surface conduction effects must be considered in the estimate of porosity from formation factor. The neutron probe appears to be sufficiently sensitive, but care must be taken to remove the effects of mafic minerals. The reasonable results obtained with the acoustic probe are encouraging but may be fortuitous. The gamma-gamma probe used in this study requires an order-of-magnitude increase in sensitivity to respond to one percent porosity variations.

Fracture Detection. The acoustic log is the most promising for the detection of fractures in igneous rock, but it should be augmented by probes responsive to borewall roughness, such as differential resistance, sensitive caliper, or televiewer (not used in this study). Compressional wave transit times respond to the major fracture zones encountered at 200 m true vertical depth, and interference patterns in the shear wave portion of the waveform respond at other zones where the compressional arrival is not disturbed. Recent progress by others shows that amplitude data are even more definitive in fracture delineation and characterization.

In general, the logs appear as one might expect in a competent granitic rock: resistivities are high, acoustic velocity is quite comparable to laboratory values, and the bore is exceptionally smooth for the most part.

One rather suprising finding was observed at the fractured zones, however. The porosity estimates, admittedly crude, indicate that the porosity increases are on the order of a few volume percent, far greater than would occur if the fracture zones consisted of a limited number of parallel planar features. It is likely that such zones are in fact highly complex on a local scale, permitting enhanced porosity and permeability values above what would be expected from a simple parallel-plate fracture model.

For waste repository investigations, it will be desirable to extract as much information as possible from exploratory boreholes, and therefore at this stage it is desirable to run a full suite of logs. This is particularly so in igneous and metamorphic rock, where the experience base is less than in sediments. A critical feature such as a fracture or dike is more readily diagnosed if more than one log respnds to that feature. Similarly, an anomalous response on one log due to an unusual or unexpected cause can very easily be misinterpreted unless contradictory or confirmatory evidence is available to check out the interpretation. Surprises do occur, as evidenced by the extraordinary gamma-ray response mentioned earlier, caused by radon migration in groundwater. The long periods of use anticipated for repositories make it important to carefully establish the true baseline conditions.

ACKNOWLEDGMENTS

REFERENCES

Brace, W.F. 1980. "Permeability of Crystalline and Argillaceous Rocks," Int. J. Rock Mech. Min. Sci. & Geomech. vol. 17, pp. 241-251.

Brace W.F. and A.F. Orange. 1968. "Further Studies of the Effects of Pressure on Electrical Resistivity of Rocks," J. Geophys. Res., vol. 74(16), pp. 5407-5420.

Brace, W.F., A.S. Orange, and T.R. Madden. 1965. "The Effect of Pressure on the Electrical Resistivity of Water Saturated Crystalline Rocks," Jour. Geophys. Research, vol. 70, no. 22, pp. 5669-5678.

Dzeban, I.P. 1970. "Elastic Wave Propagation in Fractured and Vuggy Media," Earth Physics, no. 10, pp. 31-38.

Fritz, P., J.F. Barker, and J.E. Gale. 1979. Geochemistry and Isotope Hydrology of Groundwaters in the Stripa Granite: Results and Preliminary Interpretation. Lawrence Berkeley Laboratory report LBL-8285, SAC-12, University of California, Berkeley.

Glenn, W.E. and P.H. Nelson. 1979. "Borehole Logging Techniques Applied to Base Metal Ore Deposits," in Geophysics and Geochemistry in the Search for Metallic Ores, P.J. Hood, ed. Geological Survey of Canada, Economic Geology Report 31, Ottawa, Canada, pp. 273-294.

Keys, W.S. and L.M. MacCary. 1971. "Applications of Borehole Geophysics to Water-Resources Investigations," Chapter E1 in Techniques of Water-Resource Investigations of the United States Geological Survey. U.S. Geological Survey, Washington, D.C.

King, M.S., M.R. Stauffer, and B.I. Pandit. 1978. "Quality of Rock Masses by Acoustic Borehole Logging," Proceedings of the III International Congress, I.A.E.G., pp. 156-164, Sept.

Magnusson, K. and O. Duran. 1978. Permeabilitetsbestamnigar and Geofysik Borholsmatning. KBS (Karn-Bransle-Sakerhet) Teknisk rapport 61, Stockholm.

Nelson, P.H. and W.E. Glenn. 1975. "Influence of Bound Water on the Neutron Log in Mneralized Igneous Rocks," Soc. Prof. Well Log Analysts, 16th Annual Logging Symposium, June.

Nelson, P., B. Paulsson, R. Rachiele, L. Andersson, T. Schrauf, W. Hustrulid, O. Duran, and K. Magnusson. 1979. Preliminary Report on Geophysical and Mechanical Borehole Measurements at Stripa. Lawrence Berkeley Laboratory report LBL-8280, SAC-16, University of California, Berkeley, California.

Nelson, P.H., R. Rachiele, and A. Smith. 1980. The Effect of Radon Transport in Groundwater upon Gamma Ray Borehole Logs", Lawrence Berkeley Laboratory report LBL-11180, SAC-30, University of California, Berkeley, California.

Norton, D. and R. Knapp. 1977. "Transport Phenomena in Hydrothermal
    Systems: The Nature of Porosity", Am. J. of Science, vol. 277, pp. 913-936.

Paillet, F.L. 1980. "Acoustic Propagation in the Vicinity of Fractures
    which Intersect a Fluid-Filled Borehole," Soc. Prof. Well Log Analysts 21st
    Annual Logging Symposium, Houston, Texas, pp. DD1-33.

Paulsson, B.N.P. and M.S. King. 1980. "A Cross-hole Investigation of a
    Rock Mass Subjected to Heating," Int. J. of Rock Mech. Min. Sci., in
    press.

Paulsson, B.N.P., P.H. Nelson and P. Kurfurst. 1980. Characterization
    of Discontinuities in the Stripa Granite--Full-Scale Heater Experiments,
    Lawrence Berkeley Laboratory report LBL-9063, SAC-36, University of
    California, Berkeley, California.

B. Sjogren, A. Ofathus, and J. Sandberg. 1979. "Seismic Classification of
    Rock Mass Qualities," Geophysical Prosepcting, vol. 27, no. 2, June,
    pp. 409-442.

Waxman, M.H. and L.J.M. Smits. 1968. "Electrical Conductivities in Oil-
    Bearing Shaly Sands," Soc. Petr. Eng. Jour., June.

Witherspoon, P.A., N.G.W. Cook and J.E. Gale. 1980. Progress with Field
    Investigations at Stripa. Lawrence Berkeley Laboratory report
    LBL-10559, SAC-27, University of California, Berkeley, California.

Wollenberg, H.A., S. Flexser and L. Andersson. 1980. Petrology and Radiology
    of the Stripa Pluton. Lawrence Berkeley Laboratory report LBL-11654,
    SAC-36, University of California, Berkeley, California.

APPENDIX: DESCRIPTION OF BOREHOLE PROBES

The measurement technology for borehole investigations is now well described in various engineering journals and symposia proceedings. A monograph by Keys and MacCary (1971) describes at length the principles of the measurement methods which we have used in our investigations. The following paragraphs summarize the specifications of the probes used in our investigations at Stripa. More detailed descriptions are given in reports by Nelson et al. (1979) and Magnusson and Duran (1978).

These specifications in no way imply that any of the probes is optimized for repository site characterization work. For the most part, the probes used were either readily available commercially or else where a prototype developmental version. Each could be improved in some way for better sensitivity, spatial resolution, or information content.

Gamma-ray

Both the LBL and SGU gamma-ray probes use NaI(Tl) detectors. No spectal discrimination was employed, so the total count is sensitive to the gamma-emitting radioisotopes of potassium and the decay series of uranium and thorium which are normally found in crystalline rock.

Neutron-thermal neutron

The neutron probe (o.d. 32 mm, length 1.5 m) uses a 1.4 Curie Am-Be source and a He-3 detector spaced approximately 20 cm apart. The probe was calibrated in a cubic block of granite one meter on a side perforated with small diameter holes permitting amounts of water up to 3% of the rock volume to be added. The calibrations established an effective radius of investigation of approximately 0.4 m in low porosity rock. The sensitivity to water

changes was found to be -85 counts per second per one volume percent increase in water content.

Gamma-gamma (density)

The gamma-gamma probe (o.d. 31 mm, length 2.5 m) uses a 16 milliCurie source of Am-241. The probe was designed to detect thin beds in sedimentary sequences using a single gamma-ray detector located immediately above the source such that the effective spacing is about 57 mm. In operation the probe is held against the borewall with a motorized decentralizer arm. Spatial resolution appears to be about 40 mm. Based on measured core density ρ (gm/cm^3) and log response I (counts/sec), the response equation is logI = -0.344ρ + 3.305.

Sonic velocity and waveform

The sonic velocity probe (o.d. 60 mm, length 1.4 m) uses a magneto-strictive source and piezoelectric receiver spaced 0.3 m apart. The transit time of the first compressional wave arrival was recorded analog at an absolute accuracy of about 3 microseconds and a relative accuracy of 1 microsecond. A waveform log was recorded on film in variable density format using a scale of 20 microseconds per cm on the oscilloscope face.

Caliper

The caliper probe (o.d. 51 mm., length 1.2 m) measures fluctuations in the borehole diameter by sensing the displacement of three mechanical arms linked to a linear potentiometer. A special set of short arms was acquired especially for use in the 76-mm boreholes, affording a great improvement in sensitivity. The resolution of the caliper, determined from a machined calibrator, was about 0.2 mm diametral change, a limitation imposed by the

potentiometer. Sensitivity to vertical aperture has not been established but is limited by the radius of curvature of the arm tips. Hysteresis, or the ability to track the diameter as the arms are closing or opening, is about 0.3 mm.

Differential resistance

The differential resistance probe measures the changes in resistance between a pair of electrodes spaced 12 mm apart. Since the borehole fluid furnishes the conductive path, the probe behaves qualitatively as a caliper, with small borehole enlargements decreasing the resistance between the electrodes. The probe sensitivity is enhanced is the annulus between the insulating guard and the borewall is as small as possible, preferably a fraction of a millimeter. Fractures simulated in a non-conducting plastic tube shows that the tool can detect fractures of 1 mm aperture and 1 mm depth.

Resistivity

Electrical resistivity is measured with a set of three electrode arrays; a normal array with a 1.6 m spacing, and two lateral arrays with 1.65 m and 1.05 m spacing. To avoid induction effects, a switching frequency of 0.25 Hz is used.

Self-potential

Self-potential is measured between a borehole electrode and a surface electrode. Both electrodes are non-polarizing copper-copper sulphate electrodes.

Induced Polarization

A time-domain system measures the ratio of the integrated voltage in the 0.24 - 0.48 second window to the applied voltage. The excitation pulse length is 1.96 seconds. The probe consists of two potential electrodes and a current electrode at the top. Electrode spacing is 5 m. A remote current electrode is placed on surface about 50 m from the borehole. The potential electrodes are non-polarizing copper-copper sulphate.

VLF

The VLF receiver is tuned to station GBR in England which broadcasts at 16 kHz. The ferrite core antenna measures the vector component of the magnetic field aligned along the borehole axis. A second antenna on the surface provides a reference signal for resolving real and imaginary components.